Available online at www.sciencedirect.com
SCIENCE DIRECT®
International Journal of Heat and Fluid Flow 25 (2004) 986–995
International Journal of HEAT AND FLUID FLOW
www.elsevier.com/locate/ijhff

Two-fluid mixing in a microchannel

Ying Zheng Liu [a,b], Byoung Jae Kim [b], Hyung Jin Sung [b,*]

[a] School of Mechanical Engineering, Shanghai Jiao Tong University, 1954, Huashan Road, Shanghai, 200030, PR China
[b] Department of Mechanical Engineering, Korean Advanced Institute of Science and Technology, 373-1, Guseong-dong, Yuseong-gu, Daejeon, 305-701, South Korea

Received 11 March 2003; accepted 26 March 2004
Available online 1 July 2004

Abstract

A numerical study of the mixing of two fluids (pure water and a solution of glycerol in water) in a microchannel was carried out. By varying the glycerol content of the glycerol/water solution, the variation in mixing behavior with changes in the difference in the properties of the two fluids (e.g., viscosity, density and diffusivity) was investigated. The mixing phenomena were tested for three micromixers: a squarewave mixer, a three-dimensional serpentine mixer and a staggered herringbone mixer. The governing equations of continuity, momentum and solute mass fraction were solved numerically. To evaluate mixing performance, a criterion index of mixing uniformity was proposed. In the systems considered, the Reynolds number based on averaged properties was $Re = 1$ and 10. For low Reynolds number ($Re = 1$), the mixing performance varied inversely with mass fraction of glycerol due to the dominance of molecular diffusion. The mixing performance deteriorated due to a significant reduction in the residence time of the fluid inside the mixers.

Keywords: Two-fluid mixing; Microchannel; Molecular diffusion

1. Introduction

Two-fluid mixing is an essential process in many microfluidic devices. For example, various biomedicial and biochemical processes involve the mixing of two fluids, including DNA purification, polymerase chain reaction (PCR), enzyme reaction, and protein folding. The performance of such processes relies on effective and rapid mixing of samples and reagents. Fluid properties such as density, viscosity and diffusivity vary with changes in variables such as temperature and mass fraction of species; hence, these variations should be taken into account when evaluating the extent to which two fluids mix.

Most previous experimental studies on two-fluid mixing in microfluidic devices have used flow visualization to probe the mixing performance. Koch et al. (1999) used red and green inks dissolved in ethanol to test a lateral micro mixer. Liu et al. (2000) and Beebe et al. (2001) used solutions of phenolphthalein and sodium hydroxide dissolved in ethyl alcohol to test the mixing performance of a three-dimensional serpentine mixer. Lee et al. (2000) and Stroock et al. (2002) used distinct streams of a fluorescent and a clear solution to test the mixing performance of an active mixer with a pressure source/sink system and of a staggered herringbone mixer. However, few studies have been performed to elucidate the variation in mixing behavior with changes in the difference in the properties of two fluids.

It is known that the flow inside microchannels is usually laminar ($Re < 100$) and limited by molecular diffusion (Schwesinger et al., 1996). Such flows cannot be made turbulent by placing obstacles inside the microchannel (Giridharan et al., 1999). In addition, the mechanical stirring methods usually employed in macromixers can not be implemented in microchannels due to size limitations and fabrication difficulties. Two techniques have been mainly adopted to enhance mixing inside microchannels: active and passive mixing. Active mixing entails the exertion of an external perturbation on the fluids, for example by using moving parts or a varying pressure gradient (Evans et al., 1997; Lee et al.,

* Corresponding author. Tel.: +82-42-869-3027; fax: +82-42-869-5027.
E-mail address: hjsung@kaist.ac.kr (H.J. Sung).

0142-727X/$ - see front matter © 2004 Elsevier Inc. All rights reserved.
doi:10.1016/j.ijheatfluidflow.2004.03.006

Nomenclature

Re	Reynolds number
m_g	mass of glycerol [kg]
m_w	mass of water [kg]
u	velocity component in x direction [m/s]
v	velocity component in y direction [m/s]
w	velocity component in z direction [m/s]
$\vec{V}$	velocity vector in x–y–z domain [m/s]
I_{max}	maximum intensity value of pixels
I_{mean}	average intensity value of pixels
C	criterion index of mixing uniformity normalized by I_{max}
C_{dev}	criterion index of mixing uniformity normalized by I_{mean}
C_{dev_inlet}	C_{dev} value at inlet
C_{dev_outlet}	C_{dev} value at outlet
C_{mix}	criterion index of mixing uniformity normalized by inlet C_{dev}
N	total number of pixels
i	pixel number
n	gray bit number
D	diffusivity [kg/m s]
L	streamwise length [m]
D_h	hydraulic diameter [m]

Greeks

ϕ	mass fraction of glycerol in fluid
ρ	density [kg/m^3]
μ	dynamic viscosity [kg/m s]

Superscripts

$\bar{}$	average value of two fluids

2000). Active mixing tends to be rapid and controllable, with full mixing being achieved in a short time (Jones and Aref, 1998; Lee et al., 2000). However, the fabrication, operation and maintenance of active mixers in microfluidic systems has proved difficult. In contrast, passive mixers of simple geometry have shown great potential. Various passive micromixers based on chaotic advection (Aref, 2002) have been proposed. Liu et al. (2000) designed a three-dimensional serpentine microchannel with a 'C-shaped' repeating unit to induce chaotic advection, and showed that this design enhanced fluid mixing. Bertsch et al. (2001) proposed a micromixer made of intersecting channels and a micromixer made of right- and left-handed helical elements. The geometries of these micromixers were very close to those of conventional large-scale static mixers used in the chemical and food-processing industries. Recently, Stroock et al. (2002) achieved effective and rapid mixing at $Re = 10^{-2}$–10 using a staggered herringbone mixer in which staggered and asymmetric grooves are placed on the floor of a straight channel at an oblique angle to the long axis of the channel. In the work of Stroock et al., transverse flows, which enhanced chaotic advection, were generated by means of a steady axial pressure gradient.

In the present study we examine the influence of difference in the properties of two mixing fluids on the mixing behavior. The mixing of two miscible fluids—pure water and a solution of glycerol in water—was studied numerically. In the systems studied, the difference in the properties of the two mixing fluids was adjusted by varying the amount of glycerol in the glycerol/water solution. Specifically, we varied the mass fraction of glycerol in water, $\phi = m_g/(m_g + m_w)$, where m_g and m_w are the masses of glycerol and water in the mixed solution, respectively. The density, viscosity and diffusivity of the glycerol solution were functions of ϕ. The mixing performance of the two liquids was tested in two types of micromixer: a three-dimensional serpentine mixer and a staggered herringbone mixer. The mixing of the two fluids inside these micromixers was simulated at $Re = 1$ and 10. For comparison purposes, the mixing behavior of glycerol and water in a squarewave mixer was also tested. A criterion index (a measure of mixing uniformity), C_{mix}, was proposed to evaluate mixing performance. The variation in C_{mix} with changes in ϕ, and therefore changes in the fluid properties, was examined. Three values of ϕ were chosen in the present study, $\phi = 0$, 0.2 and 0.4. We found that the mixing performance at low Reynolds number ($Re = 1$) varied inversely with mass fraction of glycerol due to the dominance of molecular diffusion. The mixing performance deteriorated due to a significant reduction in the residence time of the fluid inside the mixers. For large Reynolds number ($Re = 10$), the opposite trend was observed for the serpentine mixer, which was attributed to the enhancement of flow advection at large ϕ. However, the expected enhancement of chaotic advection with increasing Re was not found in the staggered herringbone mixer.

2. Numerical method

Flows in which two fluids, pure water and a solution of glycerol in water in the present case, are mixing can be simulated by solving the following general transport equation (Cussler, 1997):

$$\nabla \cdot [\rho(\phi)\phi\vec{V}] = \nabla \cdot [D(\phi)\nabla\phi], \tag{1}$$

where ρ is density of mixture, D is mass diffusivity, $\vec{V}$ is the velocity vector. As mentioned earlier, ϕ is the mass fraction of glycerol in the fluid.

$$\phi = m_g/(m_g + m_w), \tag{2}$$

where m_g and m_w are the masses of glycerol and water in the mixed solution, respectively. A Neumann boundary condition is applied at the solid surface and outlet.

The governing equations of continuity and three-dimensional momentum can be expressed as follows:

$$\nabla \cdot [\rho(\phi)\vec{V}] = 0, \tag{3}$$

$$\nabla \cdot [\rho(\phi)\vec{V}u] = -\frac{\partial p}{\partial x} + \nabla \cdot [\mu(\phi)\nabla u], \tag{4}$$

$$\nabla \cdot [\rho(\phi)\vec{V}v] = -\frac{\partial p}{\partial y} + \nabla \cdot [\mu(\phi)\nabla v], \tag{5}$$

$$\nabla \cdot [\rho(\phi)\vec{V}w] = -\frac{\partial p}{\partial z} + \nabla \cdot [\mu(\phi)\nabla w]. \tag{6}$$

where u, v and w are the velocity components in x, y and z directions, respectively, μ is dynamic viscosity of the fluid. During the mixing of two fluids, we would like to express the properties of the fluid mixture as functions only of ϕ; however, Eqs. (1), (3)–(6) are fully coupled with different properties. To decouple these correlations, the equations of continuity and momentum based on initially assumed ϕ, $\mu(\phi)$ and $D(\phi)$ fields were solved first, and then the transport equation of each species based on the intermediate velocity field and $D(\phi)$ was solved. The properties $\rho(\phi)$, $\mu(\phi)$ and $D(\phi)$ were updated by the calculated ϕ field. All the equations were iteratively solved by the above procedure.

In order to solve the above system of equations, the well-established numerical solution technique, SIMPLEC algorithm of Van Doormaal and Raithby (1984), was employed. In the present computations, typically 200–1200 iterations were required for the local variables to achieve convergence. For convergence criteria, the relative variation of ϕ between two successive iterations was smaller than the pre-assigned accuracy level of 10^{-4}. The spatial mesh points were typically 20×45 in height and width of the cross-sectional domain. The total computational cells of the squarewave mixer, three-dimensional serpentine mixer and staggered herringbone mixer were 0.75, 0.98, and 1.42 million, respectively. The sensitivity of the calculated results to the grid interval and accuracy level in the convergence criteria was checked by repeating calculations. The computational parameters chosen in the present work were found to yield satisfactory results in the grid convergence test.

The changes in the viscosity and diffusivity of the water–glycerol mixture (Cohen et al., 2000) with increasing ϕ are shown in Fig. 1. Both the diffusivity and viscosity of the mixture are very sensitive to ϕ, with the diffusivity decreasing and the viscosity increasing with increasing ϕ. The diffusivity varies approximately inversely with viscosity, showing a large drop on going from the dilute ($\phi = 0$) to the concentrated solution.

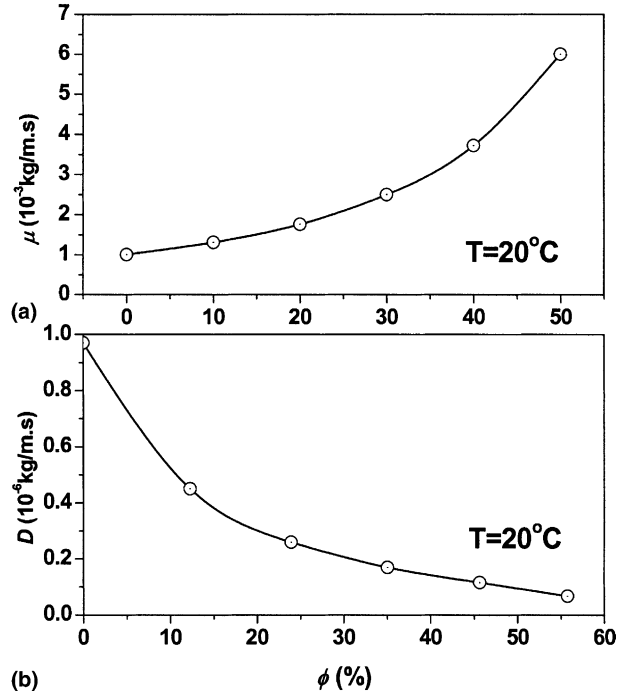

Fig. 1. Dependence of viscosity and diffusivity of mixture on mass fraction of glycerol: (a) viscosity; (b) diffusivity.

Schematic diagrams of the squarewave mixer, three-dimensional serpentine mixer and staggered herringbone mixer are shown in Figs. 2–4. The cross-sectional sizes of these mixers were 300×150 μm, 300×150 μm and 360×139 μm, respectively. The hydraulic diameters (D_h) of the inlet cross-sections were the same for all three micromixers ($D_h = 200$ μm). For the staggered herringbone mixer, the original design of Stroock et al. (2002),

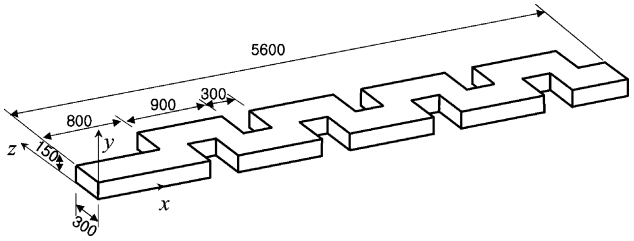

Fig. 2. Geometry of squarewave mixer (μm).

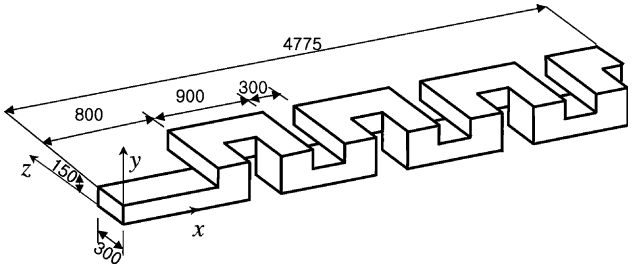

Fig. 3. Geometry of three-dimensional serpentine mixer (μm).

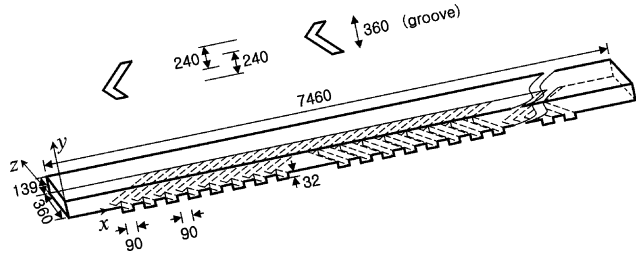

Fig. 4. Geometry of staggered herringbone mixer (μm).

in which $D_h = 111$ μm, was rescaled such that $D_h = 200$ μm to facilitate comparison with the other two micromixers. Equal volume streams of two fluids were injected into the micromixers at the same condition: one fluid was glycerol dissolved in water and the other one was pure water.

3. Evaluation criterion of mixing performance

We now define the criterion that will be used to quantify mixing performance. In the past, the criterion for the performance of two-fluid mixing inside micromixers has been usually the uniformity of the concentrated intensity of the solute. Liu et al. (2000) assessed two-fluid mixing inside a three-dimensional serpentine micromixer through measurements of the deviation of the pixel intensity values I_i in a given image from the maximum intensity value I_{max}:

$$C = \sqrt{\frac{1}{N}\sum_{i=1}^{N}(I_i - I_{max})^2}, \tag{7}$$

where N is the total number of the pixels. This criterion index should be normalized to allow comparisons between images with gray levels of different amplitudes. Two such normalized criteria are the normalized average intensity (Kim et al., 2002) and the standard deviation of intensity distribution (Stroock et al., 2002), which have been used previously to evaluate the mixing performance of a two-branch serpentine mixer and a staggered herringbone mixer, respectively.

In the present study, we chose the averaged intensity I_{mean} as the reference of mixing uniformity in order to better describe the mixing uniformity. Hence, we define a modified criterion index C_{dev} normalized by the gray level amplitudes:

$$C_{dev} = \frac{\sqrt{\frac{1}{N}\sum_{i=1}^{N}(I_i - I_{mean})^2}}{2^n - 1}, \tag{8}$$

where n is the gray bit number of the image under analysis. To compare the mixing performance achieved by different mixers under a range of conditions, a distribution of ϕ at the inlet cross-section is considered, and C_{dev} is normalized as follows to give the final criterion index, C_{mix}.

$$C_{mix} = \frac{(C_{dev\_inlet} - C_{dev\_outlet})}{C_{dev\_inlet}}, \tag{9}$$

where C_{dev_inlet} and C_{dev_outlet} are values of C_{dev} at the inlet and outlet cross-sections, respectively. If two fluids are fully mixed in the channel, the intensity I_i in Eq. (8) is the same for every pixel, and consequently C_{mix} is equal to 1. If there is no mixing at all, C_{mix} is equal to 0.

4. Results and discussion

As mentioned earlier, to make a direct comparison of the mixing performance of three mixers, the same hydraulic diameter ($D_h = 200$ μm) was employed. Moreover, we considered the same streamwise length ($L = 8000$ μm) for the three mixers, not the geometric length. Here, the streamwise length is defined as the total length where fluid flows through the mixer. For the herringbone mixer, the depth of the small staggered and asymmetric grooves was included for the total streamwise length (L). Accordingly, the streamwise length (L) is slightly larger than the geometric length. The characteristic Reynolds number is defined as $Re = \bar{\rho}\bar{u}D_h/\bar{\mu}$, where $\bar{u}$ is the mean velocity at the inlet, and $\bar{\rho}$ and $\bar{\mu}$ are the average density and viscosity of the two fluids, respectively.

First, we carried out numerical simulations of the mixing of two fluids with zero gradient of ϕ at $Re = 1$ and 10. In fact, ϕ was set to 0.001 in these calculations, but hereafter is assumed to be zero. Hence, the density, viscosity and diffusivity of the two fluids were assumed to be the same and to be constant during mixing. This assumption is commonly adopted for numerical testing of micromixers (Greiner et al., 2000). The mixing uniformities at different cross-sections in the three types of micromixer are shown in Fig. 5. This figure clearly shows that the three-dimensional serpentine mixer and staggered herringbone mixer mix the liquids to a greater extent than does the squarewave mixer. Thus, only the former two micromixers were analyzed further. To investigate the dependence of mixing performance on ϕ, three mixing cases are considered ($\phi = 0$, 0.2 and 0.4).

We now consider the two-fluid flow inside the three-dimensional serpentine mixer at $Re = 1$ and $\phi = 0$, 0.2 and 0.4. Fig. 6 shows the variation in mixing uniformity with distance through the mixer at the three values of ϕ. The mixing uniformity decreases with increasing ϕ, with the discrepancy in mixing uniformity for systems with different ϕ becoming larger as the fluids move downstream. Fig. 7 shows cross-sectional visualizations of the flows in the mixing of the systems with $\phi = 0$, 0.2 and 0.4 at various downstream distances. As shown in Fig. 7, the mixing behavior of the glycerol-containing solution

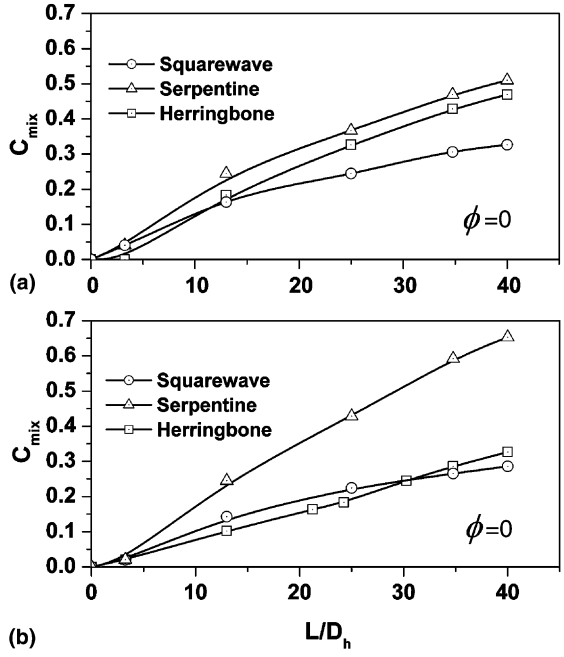

Fig. 5. Mixing performance comparison of three micromixers at $\phi = 0$: (a) $Re = 1$; (b) $Re = 10$.

(the top fluid) at each cross-section is similar at the three values of ϕ. The glycerol-containing solution is quickly rotated in the first serpentine unit, and then appears as a thumb shape. In the subsequent serpentine units, the glycerol-containing solution enlarges further into the other fluid (pure water) until the solute is advected and

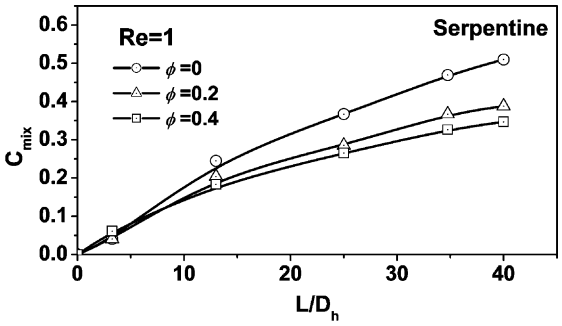

Fig. 6. Mixing performance of three-dimensional serpentine mixer at $Re = 1$.

diffused to the bottom at $L/D_h = 25$. In the straight channel, the glycerol-containing solution slows down due to its higher viscosity. The occupation of more space by the glycerol-containing solution at higher ϕ has the effect of pushing the bottom fluid, increasing its flow velocity. As the value of ϕ increases at inlet, the deformation of the slowly moving thumb-shaped configuration of the glycerol-containing solution becomes more pronounced. The interface between two fluids is then enlarged at every cross-section of the serpentine channel.

The increase in interface size with increasing ϕ at the outlet can also be seen in Fig. 8, which shows the positions of particle tracers placed at two-fluid interface for systems with $\phi = 0$, 0.2 and 0.4. In this figure, y and z correspond to the depth and width from the bottom left corner of the mixing photograph, and the inlet

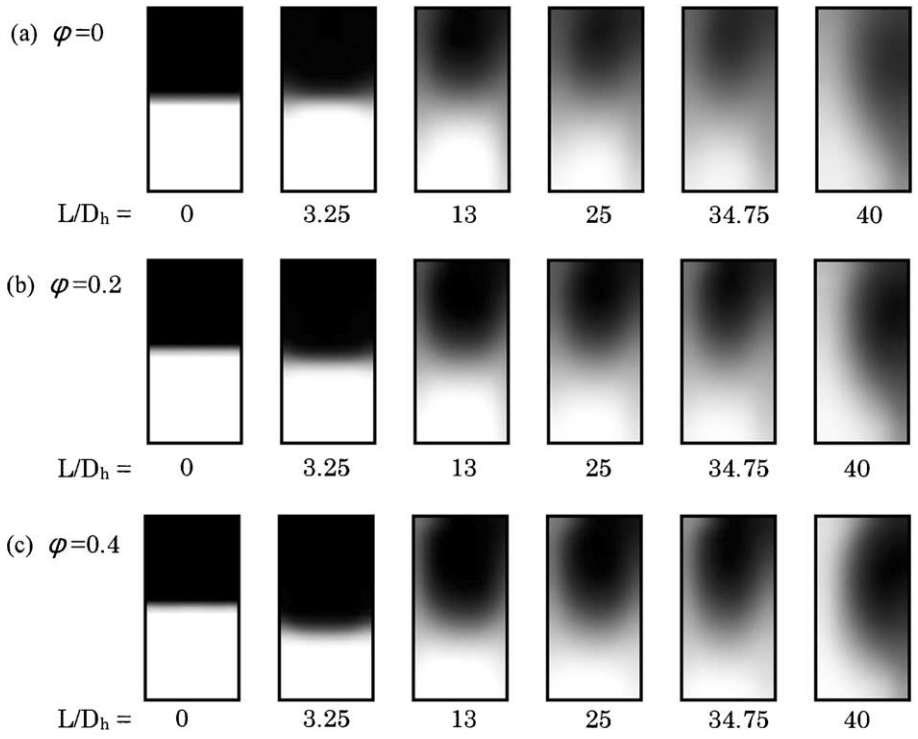

Fig. 7. Cross-section mixing photograph of three-dimensional serpentine mixer at $Re = 1$.

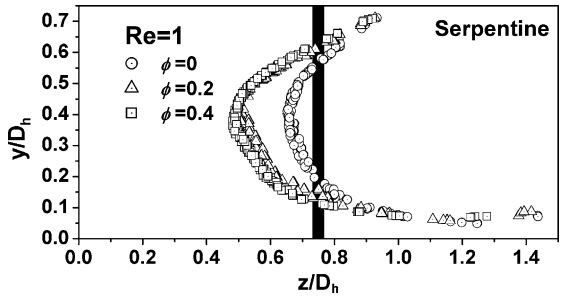

Fig. 8. Particle traces at the outlet cross-section of three-dimensional serpentine mixer at $Re = 1$.

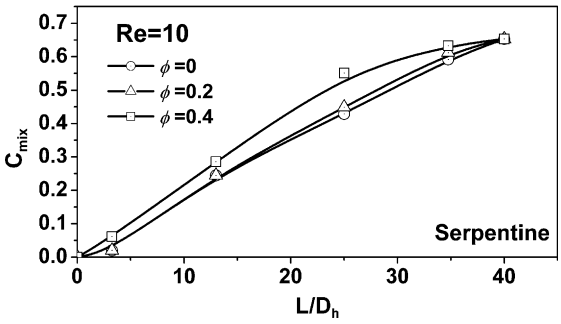

Fig. 9. Mixing performance of three-dimensional serpentine mixer at $Re = 10$.

interface between the two fluids is indicated by a thick black line, which is the same in Figs. 11, 14 and 16. After advection of fluids inside the mixer, the tracer particles are transported to the outlet cross-section. These are plotted as open symbols in Fig. 8. In the system with $\phi = 0$, the tracers are still positioned adjacent to each other in an orderly arrangement at the interface. On going to $\phi = 0.2$, however, the interface between the two fluids is substantially deflected, and is deflected slightly more when ϕ is further increased to 0.4. It is known that pure mixing of two fluids occurs through a combination of flow advection and molecular diffusion. At a fixed Re ($Re = 1$), the residence time of fluids inside the mixer decreases with increasing ϕ. Given the previous observation of no chaotic advection at $Re = 1$ (Liu et al., 2000), we conclude that molecular diffusion, which is proportional to the residence time of the fluids, is the dominant factor in two-fluid mixing inside the serpentine mixer.

The mixing behavior inside the serpentine mixer at $Re = 10$ is considered. Fig. 9 shows the mixing uniformity of the two fluids inside the mixer for systems with $\phi = 0$, 0.2 and 0.4. The mixing uniformity is higher at $Re = 10$ than at $Re = 1$ due to chaotic advection (Liu et al., 2000). However, at $Re = 10$ the mixing performance at every cross-section increases with increasing ϕ, which is the opposite of the behavior observed at $Re = 1$ (Fig. 6). The corresponding mixing is visualized in Fig. 10. The variation in mixing behavior with increasing ϕ is similar to that observed at $Re = 1$, except that the thumb-shaped configuration of the glycerol-containing solution is deformed to be very slender at $L/D_h = 13$. At

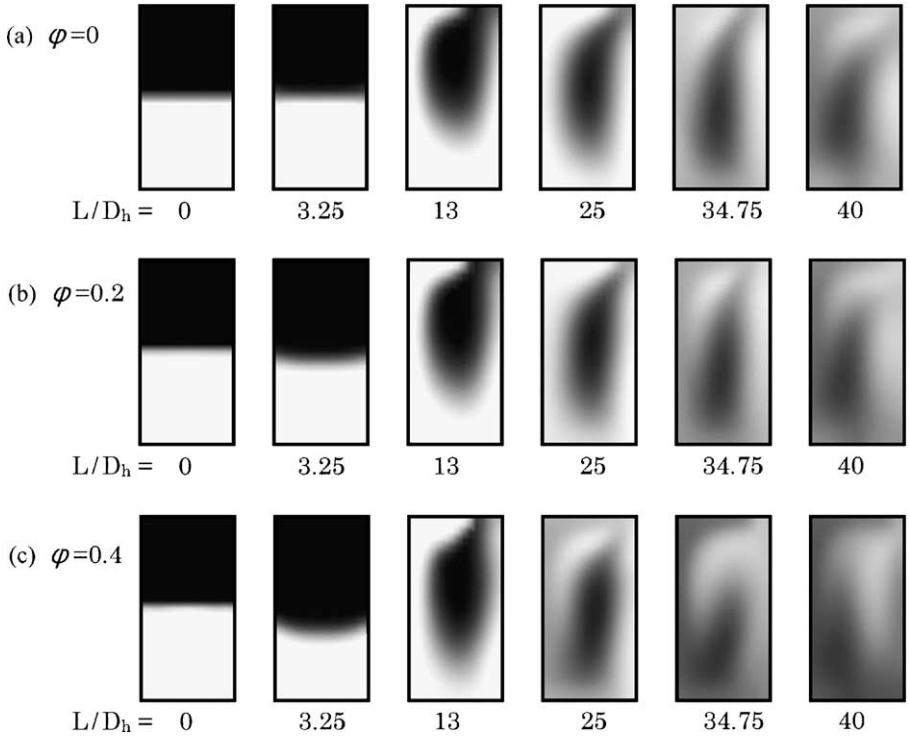

Fig. 10. Cross-section mixing photograph of three-dimensional serpentine mixer at $Re = 10$.

both $\phi = 0.2$ and 0.4, the glycerol-containing solution detaches from the top surface and moves to a central location at $L/D_h = 25$. As a result, diffusion of the solute is enhanced during deformation of the interface between the two fluids. For the $\phi = 0.4$ system, the glycerol-containing solution attaches to the bottom surface at $L/D_h = 34.75$, and the solute is distributed across the entire cross-section. At $L/D_h = 40$, the interface becomes difficult to distinguish. The effect of flow advection at $Re = 10$ is evident in Fig. 11, which shows the distribution of particle tracers at the outlet cross-section. At $\phi = 0$, the tracer particles are continuously and uniformly adjacent despite significant distortion of the interface. However, when ϕ is increased to 0.2 and 0.4, the tracers at large z deviate from their locations at $\phi = 0$. At $\phi = 0.4$, the continuously and uniformly adjacent arrangement of tracer particles is broken at the center of the interface, indicating an enhancement of flow advection. Therefore, the switch in the behavior of the mixing uniformity on going from $Re = 1$ to 10 (Figs. 6 and 9) can be attributed to a shift from the dominance of molecular diffusion at $Re = 1$ to the dominance of advection at $Re = 10$.

In an effort to understand the two-fluid mixing inside the channel, both the cross-sectional mixing photographs and corresponding velocity vectors at $L/D_h = 8.5$ are shown in Fig. 12. The position ($L/D_h = 8.5$) is near the center of the first serpentine unit. It is seen that the mixing photographs and velocity vectors for $Re = 1$ are not so much influenced by different ϕ. However, when Re is increased to $Re = 10$, the flow at the left bottom corner is enhanced with increasing ϕ. This shows an evidence of the enhanced flow advection. The enhanced secondary flow, in combination with the streamwise flow, extends to a great extent the two-fluid interfacial area across which diffusion occurs (Liu et al., 2000). Note that Beebe et al. (2001) observed the chaotic advection in the serpentine mixer. As seen in Fig. 10, the glycerol-containing fluid occupies more cross-sectional space at $L/D_h = 3.25$ than the other fluid. The other fluid is pushed to move faster inside the serpentine unit with increasing ϕ. Accordingly, the local Reynolds number of the other fluid is increased, which gives rise to the enhancement of flow advection as ϕ increases. The two-fluid interfacial area is rapidly extended as ϕ increases.

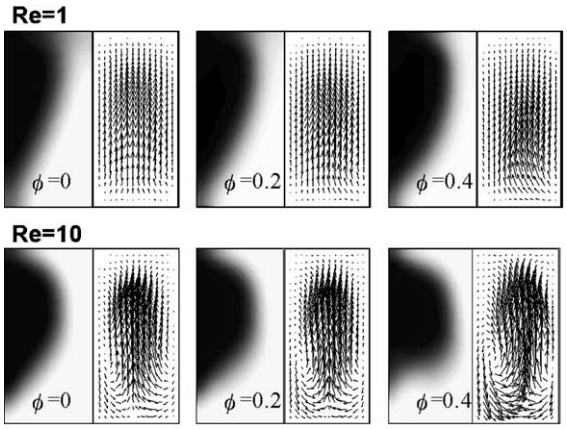

Fig. 12. Cross-section mixing photograph and cross-flow vector field of serpentine mixer at $L/D_h = 8.5$.

Next, we turn to the mixing behavior inside the staggered herringbone mixer. The variation in mixing uniformity inside the mixer on going downstream at $Re = 1$ is shown in Fig. 13. The mixing performance is slightly inferior to that of the serpentine mixer at the same Reynolds number, although the variation in mixing uniformity with increasing ϕ is very similar for the two types of mixer. Inside the herringbone mixer, the bottom grooves trigger traverse motion that gives rise to chaotic advection (Stroock et al., 2002). The mixing captured at different cross-sections is visualized in Fig. 14. At $L/D_h = 13$, the bottom fluid turns into the groove and drives the glycerol-containing solution (the top fluid) outwards. As the fluids move downstream, the asymmetric and staggered arrangement of the grooves enhances agitation of the glycerol-containing solution, which is fragmented at the outlet. When ϕ is increased to 0.2 and 0.4, the slowly moving glycerol-containing solution becomes entangled with the bottom fluid, but the gray intensity of the photographs becomes less uniform. The two-fluid interfaces are clearly discernible

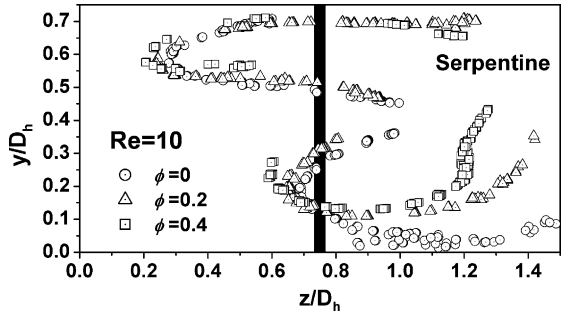

Fig. 11. Particle traces at the outlet cross-section of three-dimensional serpentine mixer at $Re = 10$.

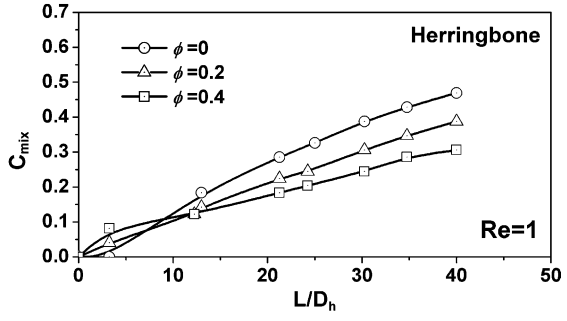

Fig. 13. Mixing performance of staggered herringbone mixer at $Re = 1$.

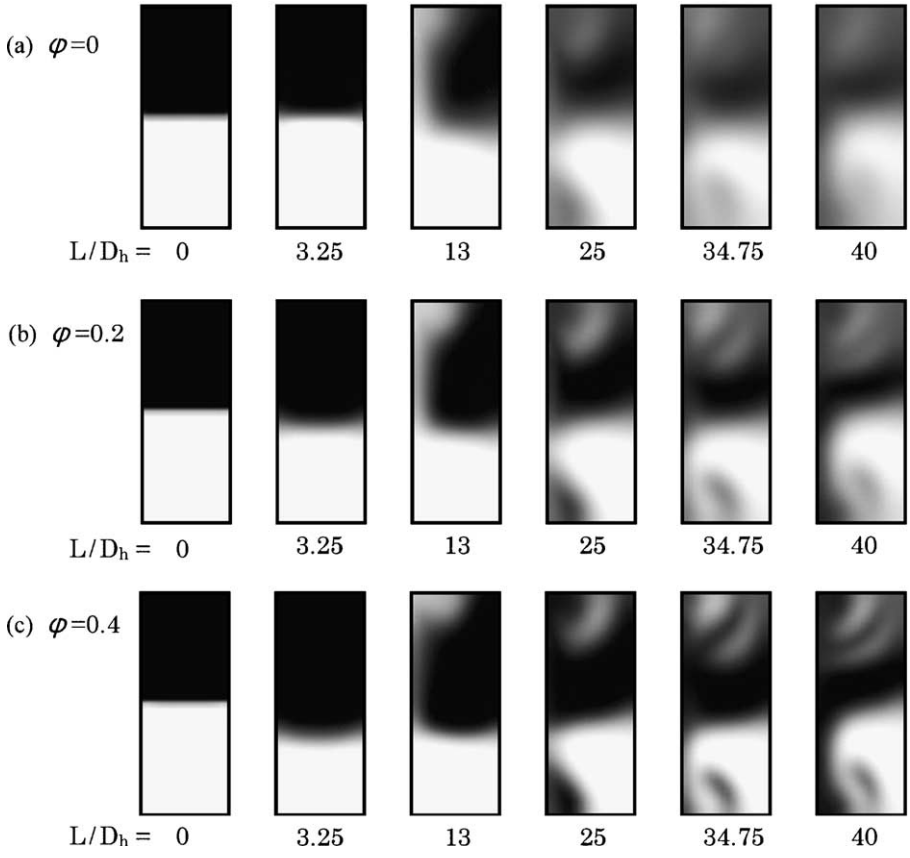

Fig. 14. Cross-section mixing photograph of staggered herringbone mixer at $Re = 1$.

compared with the case of serpentine mixer. Inspection of the distribution of tracer particles at the outlet cross-section in Fig. 15 shows that the particles maintain their positions adjacent to each other, with only slight difference on going from $\phi = 0.2$ to 0.4.

When Re is increased to 10, the trend in the mixing uniformity with changing ϕ (Fig. 16) remains similar to that at $Re = 1$ although the curves are closer together at the higher Reynolds number. Recall that the mixing performance of the herringbone mixer is slightly inferior to that of the serpentine mixer at the same Reynolds number in Figs. 6, 9, 13 and 16. The distributions of

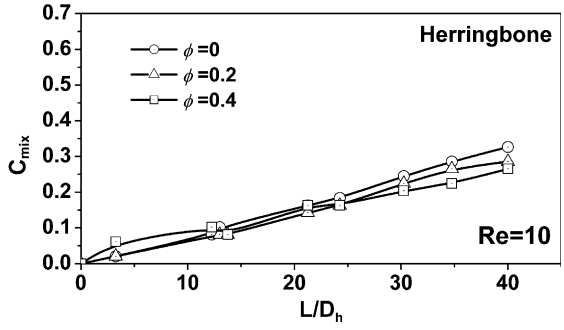

Fig. 16. Mixing performance of staggered herringbone mixer at $Re = 10$.

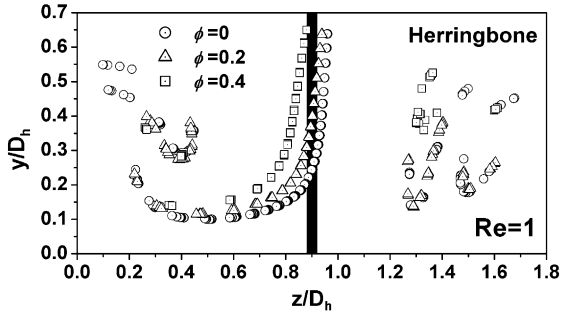

Fig. 15. Particle traces at the outlet cross-section of staggered herringbone mixer at $Re = 1$.

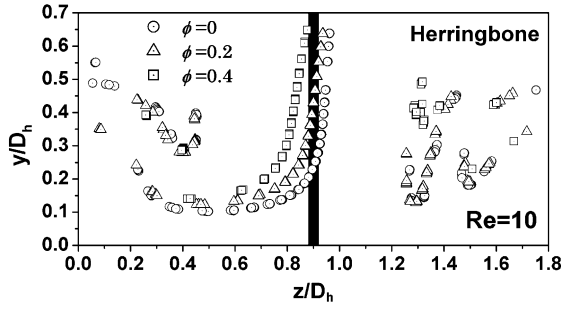

Fig. 17. Particle traces at the outlet cross-section of staggered herringbone mixer at $Re = 10$.

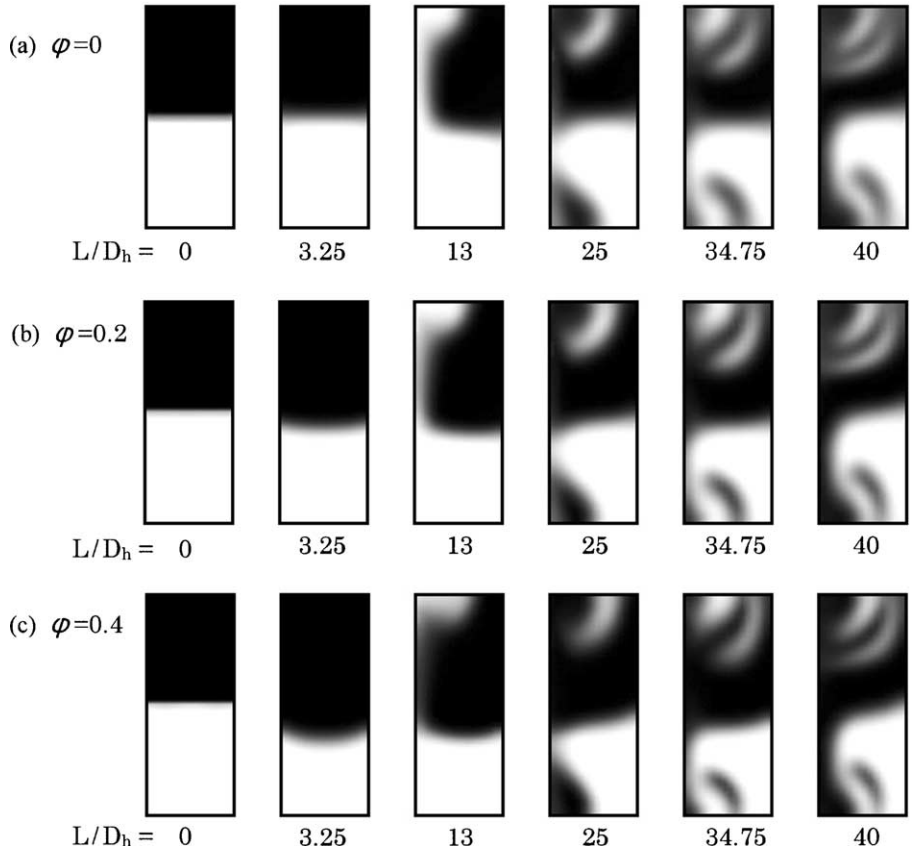

Fig. 18. Cross-section mixing photograph of staggered herringbone mixer at $Re = 10$.

tracer particles at the outlet cross-section for $Re = 10$ (Fig. 17) is basically the same as $Re = 1$. Unlike the mixing inside the serpentine mixer, flow advection inside the herringbone mixer does not show the expected enhancement when the Reynolds number is increased. From the visualizations of the mixing, shown in Fig. 18, we see that the breakdown of the glycerol-containing solution and deformation of the interface between the two fluids at $Re = 10$ is similar to that at $Re = 1$, and that it is independent of ϕ. The cross-sectional mixing photographs and velocity vectors at $L/D_h = 20$ are displayed in Fig. 19. No clear difference is found at different Re and ϕ. This indicates that the flow advection is not influenced by Re and ϕ. The flow advection inside the herringbone mixer is not enhanced as expected as Re increases. Stroock et al. (2002) also addressed that the flow field inside the herringbone mixer is independent of Re for $Re < 100$. The change of the mixing uniformity at different Re is primarily attributed to molecular diffusion.

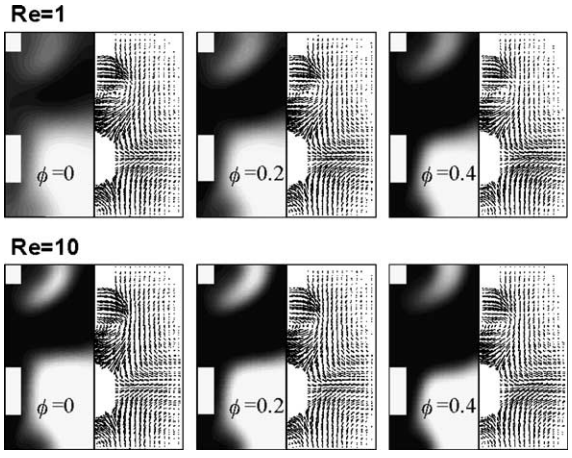

Fig. 19. Cross-section mixing photograph and cross-flow vector field of herringbone mixer at $L/D_h = 20$.

5. Conclusions

The mixing of two fluids was numerically modeled for two types of micromixer: a three-dimensional serpentine mixer and a staggered herringbone mixer. In these calculations, the mixing of pure water with a solution of glycerol in water was investigated for three different mass fractions of glycerol ($\phi = 0$, 0.2 and 0.4). These fluids were chosen to test the mixing behavior of fluids with different properties and a large concentration gradient. The dependence of the mixing performance on ϕ at $Re = 1$ and 10 was examined. At $Re = 1$, the mixing performance of both mixers varied inversely with mass fraction of glycerol due to the dominance of molecular

diffusion. When the Reynolds number was increased to 10, the opposite trend was observed for the serpentine mixer. This change in behavior was attributed to the enhancement of flow advection at large ϕ. However, no such change was observed on increasing the Reynolds number in the herringbone mixer. In fact, not only was the expected enhancement of chaotic advection absent on increasing the *Re* in the herringbone mixer, the mixing performance actually deteriorated due to a significant reduction in the residence time of the fluids inside the mixer.

References

Aref, H., 2002. The development of chaos advection. Phys. Fluids 14, 1315.

Beebe, D.J., Adrian, R.J., Olsen, M.G., Stremler, M.A., Hassan, A., Jo, B.H., 2001. Passive mixing in microchannels: fabrication and flow experiments. Mec. Ind. 2, 343.

Bertsch, A., Heimgartner, S., Cousseau, P., Renaud, P., 2001. 3D micromixers-downscaling large scale industrial static mixers. In: Proc. IEEE MEMS, Interlaken, Switzerland, p. 507.

Cohen, B., Huppert, D., Agmon, N., 2000. Non-exponential Smoluchowski dynamics in fast acid–base reaction. J. Am. Chem. Soc. 122, 9838.

Cussler, E.L., 1997. Diffusion Mass Transfer in Fluid System. Cambridge University Press, 67–68.

Evans, J., Liepmann, D., Pisano, A.P., 1997. Planar laminar mixer. In: Proc. IEEE MEMS Workshop, Nagoya, Japan, p. 96.

Giridharan, M.G., Krishnamoorthy, S., Krishnan, A., 1999. Computational simulation of microfluidics, electrokinetics and particle transport in biological MEMS devices. Symp. Design, Test, and Microfabrication of MEMS/MOEMS, Paris, France.

Greiner, K.B., Deshpande, M., Gilbert, J.R., Ismagilov, R.F., Stroock, A.D., Whitesides, G.M., 2000. Design analysis and 3D measurement of diffusive broadening in a Y-mixer. Technical Proceedings of Micro Total Analysis Systems, Enschede, The Netherlands, MicroTAS, p. 87.

Jones, S.W., Aref, H., 1998. Chaotic advection in pulsed source-sink systems. Phys. Fluids 31, 469.

Kim, J.H., Kim, B.G., Nam, H., Park, D.E., Yun, K.S., Yoon, J.B., You, J., Yoon, E., 2002. A disposable DNA sample preparation microfluidic chip for nucleic acid probe assay. In: Proc. IEEE MEMS, Las Vegas, USA, p. 133.

Koch, M., Witt, H., Evans, A.G.R., Brunnschweiler, A., 1999. Improved characterization technique for micromixers. J. Micromech. Microeng. 9, 156.

Lee, Y.K., Tabeling, P., Shih, C., Ho, C.M., 2000. Characterization of a MEMS-fabricated mixing device. In: Proc. ASME IMECE, Orlando, Florida.

Liu, R.H., Stremler, M.A., Sharp, K.V., Olsen, M.G., Santiago, J.G., Adrian, R.J., Aref, H., Beebe, D.J., 2000. Passive mixing in a three-dimensional serpentine microchannel. J. MEMS 9, 190.

Schwesinger, N., Frank, T., Wurmus, H., 1996. A modular microfluid system with an integrated micromixer. J. Micromech. Microeng. 6, 99.

Stroock, A.D., Dertinger, S.K.W., Ajdari, A., Mezic, I., Stone, H.A., Whitesides, G.M., 2002. Chaotic mixer for microchannels. Science 295, 647.

Van Doormaal, J.P., Raithby, G.D., 1984. Enhancements of the simple method for predicting incompressible fluid flows. Numer. Heat Transfer 7, 147.